The effect of a tall tower on flow and dispersion through a model urban neighborhood

Part 1. Flow characteristics

David K. Heist,[a] Jennifer Richmond-Bryant,[b] Laurie A. Brixey,[c] George E. Bowker,[d] Steven G. Perry[a] and Russell W. Wiener[e]

[a]Atmospheric Sciences Modeling Division, Air Resources Laboratory, National Oceanic and Atmospheric Administration, Research Triangle Park, NC 27711, USA

[b]Environmental and Occupational Health Sciences, Hunter College, City University of New York, 425 East 25th Street, New York, NY 10010, USA

[c]Alion Science and Technology, P.O. Box 12313, Research Triangle Park, NC 27709, USA

[d]Atmospheric Modeling Division, National Exposure Research Laboratory, US Environmental Protection Agency, Research Triangle Park, NC 27711, USA

[e]National Homeland Security Research Center, US Environmental Protection Agency, Research Triangle Park, NC 27711, USA

Disclaimer

The research presented here was performed under the Memorandum of Understanding between the U.S. Environmental Protection Agency (EPA) and the U.S. Department of Commerce's National Oceanic and Atmospheric Administration (NOAA) and under agreement number DW13921548. This work constitutes a contribution to the NOAA Air Quality Program. Although it has been reviewed by EPA and NOAA and approved for publication, it does not necessarily reflect their policies or views. Mention of trade names or commercial products does not constitute endorsement or recommendation for use.

Abstract

Wind tunnel and computational fluid dynamics (CFD) studies were performed to examine the effect of a tall tower on the flow around an otherwise uniform array of buildings. The model used in both the wind tunnel and CFD studies was designed to simulate an area of Brooklyn, NY, where blocks of residential row houses form a neighborhood bordering a major urban highway.

This area was the site of a field study that, along with the work reported here, had the goal of improving the understanding of airflow and dispersion patterns within urban micro-environments. Results reveal that a tall tower has a dramatic effect on the flow in the street canyons in the neighboring blocks, enhancing the exchange between the street canyon flow and the free-stream flow aloft. In particular, vertical motion down the windward side and up the leeward side of the tower resulted in strong flows in the lateral street canyons and increased winds in the street canyons in the immediate vicinity of the tower. These phenomena were visible in both the wind tunnel and CFD results, although some minor differences in the flow fields were noted.

Introduction

Urban and suburban neighborhoods present challenges for the prediction of pollutant dispersion due to the heterogeneity of building configurations which sets up irregular, complex wind patterns. There is a need to identify and quantify the relative importance of the dominant factors that affect the dispersion. There have been many studies on regular arrays of buildings to develop an understanding of the phenomena involved in urban dispersion, focusing on such factors as street canyon width, building aspect ratio, traffic, and orientation of street canyons to prevailing winds.[1–5] These studies have produced a better understanding of the importance of near-field effects on the initial dispersion of a plume arising from an urban source within the street canyon (*e.g.*, traffic). Several recent studies[6–8] have highlighted the effect variations in building height can have on the airflow patterns in urban areas. These variations enhance the transfer of momentum from the winds aloft into the building canopy and provide for the rapid vertical mixing of the pollutant from the street canyons. In this paper we examine the effect of a single building that towers above a neighborhood of buildings of uniform height.

A combined wind tunnel and computational fluid dynamics (CFD) study was undertaken to supplement a field study performed in Brooklyn, NY, USA, designed to study the dispersion of pollutants from a line source in an urban neighborhood. This paper is the first of two papers describing flow and pollutant dispersion for an idealized scale model of the site (see also Brixey *et al.*[9]). The field study, the Brooklyn Traffic Real-Time Ambient Pollutant Penetration and Environmental Dispersion (B-TRAPPED) Study, was performed in May 2005 with the goal of improving the understanding of airflow patterns through a complex area to be able to predict the

dispersion patterns of pollution from traffic and hazardous releases along the roadway.[10–14] The section of the city chosen for the study has fairly regular city block shapes comprising row houses with uniform heights and common backyards that form a courtyard. Adjacent to the major thoroughfare passing through the study area was one tall building that dominated the area. Standing 12 stories tall, it was significantly higher than the neighborhood row houses which were typically three stories tall.

The experimental and numerical studies were performed to complement each other. The wind tunnel study can provide insight into the flow patterns throughout the study area, supplementing the information gathered from a limited number of field instruments deployed in typical field studies and providing data to compare with the results of the numerical study. The numerical study provides a more complete picture of the flow and concentration fields since the velocity and concentration fields over the whole domain are computed. The goal of this study is not, however, intended to be a comprehensive evaluation of the numerical simulation, but rather to identify important flow phenomena in urban and suburban areas identified by both techniques.

Methods

Meteorological wind tunnel experiment

Wind tunnel. The experiments were conducted in the EPA Fluid Modeling Facility's single-pass, draw-through meteorological wind tunnel (test section 3.7 m wide, 2.1 m high, and 18.3 m long).[15] The flow in the wind tunnel is conditioned to produce a deep boundary layer appropriate for simulating neutral atmospheric conditions in an urban area by a series of screens, honeycombs, and boundary-layer generation devices. These devices include three truncated Irwin spires[16] at the upwind limit of the test section that are tapered in height to remove progressively more momentum from the flow approaching the floor of the tunnel. Roughness blocks are positioned on the floor downwind of the spires to enhance the turbulence levels near the floor and maintain the boundary layer in equilibrium. In addition, the tunnel ceiling is adjustable to allow compensation for the blockage created by the model and the growth of the wall boundary layers to produce a non-accelerating freestream flow. With a freestream flow speed of 4.2 ms^{-1}, the boundary layer that develops from this system has a friction velocity, u_*, of 0.23 ms^{-1} and a roughness length, z_0, of 0.7 mm (7 cm when scaled up to full scale).

Considering the smallest street width, D, of 12 cm, the street canyon Reynolds number ($\rho U_H D/\mu$) was approximately 24,000. The freestream velocity was chosen to ensure that the Reynolds number of the flow through the model was substantially higher than 11,000, the critical number for Reynolds number independence.[17]

Neighborhood-scale model. An idealized scale model (at 1:100 scale) of the field study site (Fig. 1) in Brooklyn was placed in the wind tunnel. The neighborhood consists of rectangular city blocks each composed of attached row houses of similar heights. The row houses have adjoining backyards that form an open area in the center of each block. The domain modeled within the wind tunnel consisted of 30 city blocks arranged in a regular array of five rows of six blocks each (Fig. 2). The primary wind direction was parallel to the long axis of the blocks. The height of the model buildings (H) was 12 cm, approximately corresponding to a full-scale, three-story building. The model blocks were 4H wide and 8H long with the depth of the houses equal to that of the "courtyard" (1.33H).

Fig. 1 Aerial photograph of the neighborhood in Brooklyn, NY, studied in the B-TRAPPED field study. The 12-story tower is indicated with a white rectangle. Solid white lines mark two major avenues, corresponding to Avenue 2 (left) and Avenue 3 (right) in the wind tunnel and CFD models. The dashed white line highlights one of the streets parallel to the wind direction.

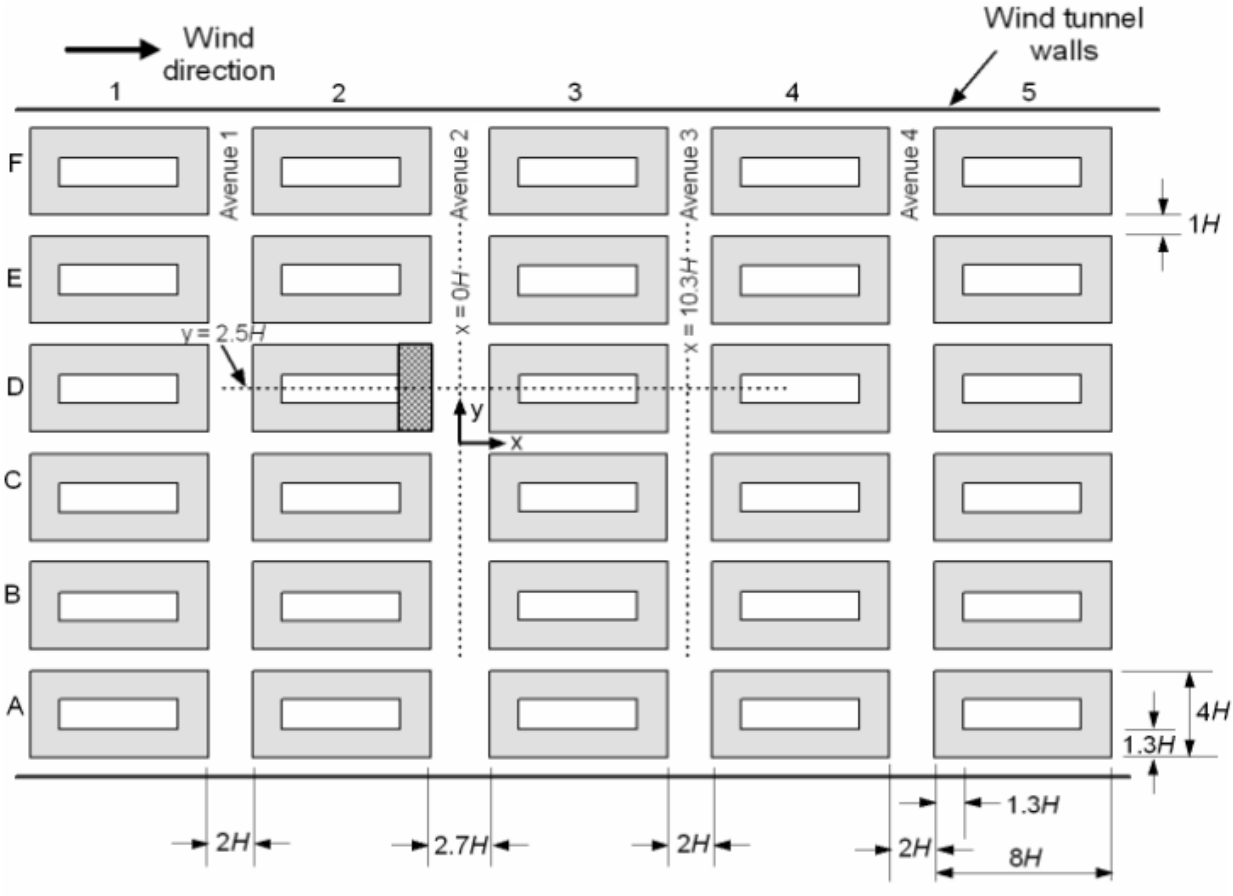

Fig. 2 Wind tunnel model city block array. The model was built at a 1:100 scale relative to full scale. Letters A through G and numbers 1 through 5 are used to indicate particular buildings in the array. Cross-hatching indicates the location of the tower.

Throughout this paper, the streamwise streets (1*H* wide) are referred to as "streets," while the cross-stream streets (typically 2*H* wide) are called "avenues" (Fig. 2). One avenue was wider than the others at 2.67*H*, simulating the width of a major urban multi-lane expressway (3rd Avenue) in Brooklyn. The source for the concentration measurements[9] is located in this wider avenue downwind of the second row of blocks.

One block was constructed of Plexiglas and had 152 ports installed for concentration and pressure measurements. This block was designed to be interchangeable with the other city blocks for acquiring building surface data at a variety of locations.

A tall tower (representing a 12-story building in the field study) was positioned at the downwind end of one of the blocks just upwind of the source (Fig. 2, block D2) to determine the

impact of this building on downwind concentrations. The tower is 1.33H long, 4H wide, and 4H tall from ground level.

Laser Doppler velocimetry. The laser Doppler velocimetry (LDV) system used in these experiments to measure velocities was a two-component, single-probe system that employed the 488- and 514.5-nm lines from a Coherent Innova 70C argon-ion laser. The beam splitting, frequency shifting, and coupling of laser light to fiber-optic cables were all accomplished using a TSI Colorburst multicolor beam separator (Model 9201, TSI Inc., St. Paul, MN, USA). The LDV system was used in the real fringe mode with a frequency shift of 40 MHz to eliminate direction ambiguity in the velocity measurements. The use of a portable fiber-optic probe (TSI Model 9832 with a 500 mm focal distance lens) facilitated movement of the LDV measurement volume, an ellipsoid with a diameter of approximately 80 μm and a length of about 1 mm. The LDV probe was installed on the wind tunnel carriage for computer-controlled positioning.

Theatrical smoke was used as seeding material for the LDV (Model 1600 fog machine, Rosco Laboratories Inc., Stamford, CT) and was introduced near the inlet of the tunnel, far upstream of the model. Data were processed with a digital burst correlator (Model IFA 755, TSI Inc.) and acquired using FIND for Windows software (version 1.4, TSI Inc.).

Pressure. Mean surface pressure measurements were made at 152 locations on the model building. These ports were constructed from brass tubing (0.16 cm inner diameter) mounted with the tube opening flush with the surface of the building. Six capacitance manometers were used during these measurements (five MKS Baratron, Model 270s with Model 698A01TRC heads and one MKS Baratron Model 170M-6C with Model 398HD-001 head, Wilmington, MA). One manometer was used to monitor the Pitot-static tube mounted at a height of 1.65 m above the floor approximately 6 m upstream of the model building. The other five were connected to building ports through a system that allowed automated switching between the 152 surface ports. The coefficient of pressure ($Cp = (P_{\text{building}} - P_{\text{static}})/(0.5\rho U_{\text{o}}^2)$) was calculated by incorporating the measurement of static pressure from the Pitot-static tube, where P_{building} is the surface measurement, P_{static} is the Pitot-static tube measurement, ρ is the air density, and U_{o} is the freestream flow velocity.

Computational fluid dynamics simulation

Geometry. The CFD model geometry shown in Fig. 3 was created using the GAMBIT v.2.1.0 (FLUENT, Inc., Lebanon, NH, USA) software. The model geometry was similar to that used in the wind tunnel, but some differences accommodate memory constraints imposed by the meshing process. The model geometry consisted of three rows of four blocks of the same dimensions as used in the wind tunnel. The building height, H = 12 m, was used for scaling. The source avenue width was slightly larger than for the wind tunnel experiments, with the first and second rows separated by a distance of 3H. The tower, having a height of 4H (from the ground), was centered at x = -2.3H and y = 2.5H, as shown in Fig. 3. x/H = 0 was designated 1.67H downstream of the first row of buildings, y/H = 0 was positioned at the center of the domain between the second and third building columns, and z/H = 0 was located at the ground. The domain limits were -23.67 < x/H < 33.67, -19 < y/H < 19, 0 < z/H < 8.

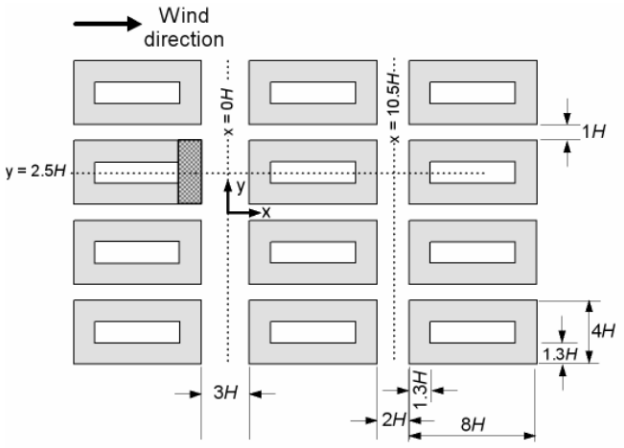

Fig. 3 CFD model layout. Cross-hatching indicates location of tower. The domain limits noted in the geometry section are not shown here.

Computational mesh. GAMBIT v.2.1.0 was also employed to create the initial mesh, and refinement of the mesh was performed within the FLUENT v.6.2.16 software. A tetrahedral mesh was employed. The mesh was graded so that mesh size was larger around the edges of the domain and refined within the vicinity of the buildings. Grid independence testing was performed according to Roache.[18] Three successively finer meshes were created, and the resultant average velocity was computed at 99 locations along y/H = 0. The error was calculated

as the L_2 norm of the velocity differences for the grid refinements normalized by the L_2 norm of the velocity. The grid convergence index (GCI) for each refinement was then computed as

$$GCI = F_S \frac{|\varepsilon|}{r^p - 1}, \quad (1)$$

where ε is relative error norm, F_S is factor of safety, r is mesh refinement factor, and p is order of the solution method. The initial mesh contained 545,088 three-dimensional elements. The mesh length scale was refined twice along regions of high-velocity gradients to produce meshes with 1,286,878 and 2,029,900 elements. Grid independence testing resulted in a GCI of 0.13 with $F_S = 3$, $r = 1.16$ [$= (2{,}029{,}900/1{,}286{,}898)^{1/3}$] to approximate the length scale of the refinement, and $p = 2$ for the second-order solution method. The GCI testing was performed with a time step of 0.05 s. The GCI indicated the error of 13% in the velocity field was a function of mesh size. Although this GCI was fairly large, another mesh refinement was prohibitive because the computer memory needed for the simulation and the computation time for the time-dependent simulation to be implemented exceeded available resources. Given the goal of the simulations to illustrate flow behavior, rather than to develop a precise velocity field, this GCI is reasonable.

Analogous to the GCI, a time-step convergence index (TCI) was created to describe the error of reducing time step on the grid-independent solution. We used the same formula as for GCI except the relative L_2 error norm computed for the finer meshes was replaced by a relative L_2 error norm for finer time steps. The refinement value, r, was then the ratio of the time-step size rather than the grid length scale. Time steps of 0.2 s, 0.1 s, and 0.05 s were tested, and a second-order solution was still assumed. Time-step independence testing demonstrated a TCI of 0.0057 for the time-step independent solution using the 2,029,900 cell mesh. This TCI indicated negligible error in the velocity field as a function of time step.

Turbulence model. The CFD simulations presented in this paper use Large Eddy Simulation (LES) to model the flow. LES is a well-documented method and has been used in a large number of street canyon studies to examine airflow characteristics in idealized canyons,[19–21] building arrays,[2,22] and complex urban geometry.[22] LES is a time-dependent simulation of the fluid velocity field. Given the computation time incurred by employing a direct numerical solution of the Navier-Stokes equations at all turbulent length scales, LES presents a compromise between a direct solution method and a method such as k~ε, which approximates the turbulent viscosity.

In FLUENT, the large-eddy scales were solved directly through a finite volume formulation of the Navier-Stokes equations over the grid spacing. The small scales of turbulence were approximated with a subgrid scale (SGS) model at length scales smaller than the grid spacing. In the SGS model, the Navier-Stokes equations were closed by a formulation of the subgrid-scale stress, τ [23–25]:

$$\tau_{ij} = \rho\overline{u_i u_j} - \rho\bar{u}_i\bar{u}_j, \tag{2}$$

where ρ is fluid density, u is velocity, and i and j denote velocity components. For low Reynolds number flows, the SGS model may be dampened in the boundary layer. For relatively high Reynolds number flows, such as the one modeled here, it was not possible to resolve the sharp flow gradient near the boundary. For this reason, logarithmic wall model approximations were used near the boundary. Initial and boundary conditions for the simulation consisted only of the incoming velocity field and the geometry. LES does not require any approximation of upstream turbulence conditions.

Boundary conditions. A logarithmic formulation of the upstream velocity profile was designated to match that used in the wind tunnel:

$$\frac{u}{u*} = \frac{1}{\kappa}\ln\left(\frac{z-d}{z_0}\right), \tag{3}$$

where u_* is friction velocity, $\kappa = 0.4$ is von Karman's constant, z_0 is roughness length scale, and d is displacement length. These parameters were selected to match the wind tunnel experiments at a 1:100 full scale equivalent ($u_* = 0.23$ m s^{-1}, $z_0 = 0.07$ m, $d = 0$ m). All solid entities, including the building surfaces and ground, had no-slip and no-flow designations to preserve mass balance.

Results and discussion

Wind tunnel measurements and numerical simulations of the flow through the building array present a picture of urban wind flow that exhibits significant channeling in the lateral avenues and strong vertical flows surrounding the tall tower. The tower in the array substantially influenced the patterns of flow throughout the building array. Vertical flow was found near the faces of the tall building, toward the ground on the windward face and upward from the ground on the leeward face. Vertical flow near the tower is important because of its ability to transport high-momentum air from the upper boundary layer into the street canyons and air from ground

level, potentially polluted from a hazardous release, up over the roof lines of the neighboring buildings. Fig. 4 shows the latter phenomenon with smoke from a pollutant source in the avenue immediately downwind of the tower transported up the lee side of the tower. The source in the photograph is a line segment source spanning an intersection and extending from the midpoint of row C to the midpoint of row D (Fig. 2). The effect of the tower on pollutant dispersion is discussed in more detail in Brixey *et al.*[9]

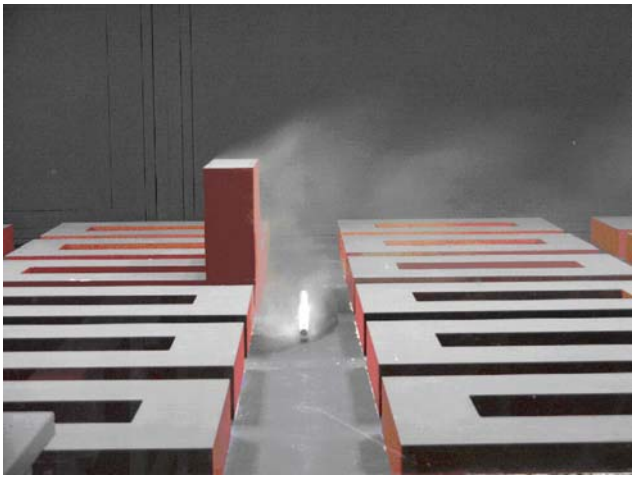

Fig. 4 Flow visualization of a line segment source in Avenue 2 demonstrating the vertical flow up the leeward side of the building. Measurements show that there is an opposite effect on the windward face of the building that produces a downdraft. Freestream flow is from left to right.

The velocity field responsible for the transport of pollutants, illustrated with flow visualization, is revealed in both the wind tunnel measurements and in the CFD simulations. Fig. 5 shows velocity vectors measured in the wind tunnel along a streamwise vertical plane intersecting the tall tower at its spanwise center (*i.e.*, at $y/H = 2.5$). As the flow approaches the tower it splits into a portion traveling over the tower and a larger portion deflected downward. This downward motion enhances the transport of momentum from the upper elevations into the street canyons. This figure also shows the dramatic upwash in the lee of the tower which begins at ground level and extends to the top of the tower. The magnitude of the vertical velocities in this area reaches 25% of the freestream velocity.

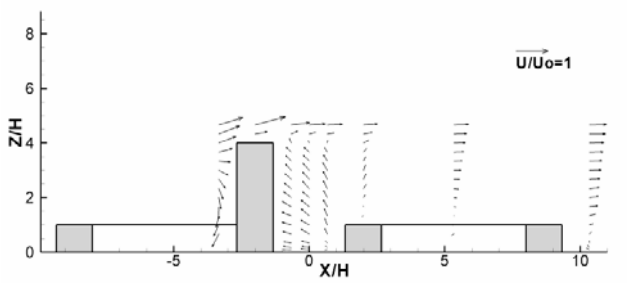

Fig. 5 Mean velocity vectors measured with LDV at *y/H* = 2.5. Freestream flow is from left to right.

The CFD results present a more detailed picture of the flow field, filling in the gaps between the velocity measurements from the wind tunnel. The CFD results show that flow upwind and downwind of the tower comprises large recirculating eddies that are horizontally centered roughly on the courtyards of the upwind and downwind city blocks as shown in Fig. 6. The figure also shows the upwash on the lee side of the tower, with CFD also indicating vertical velocities reaching 21-28% of the freestream velocity in this area, accounting for the GCI.

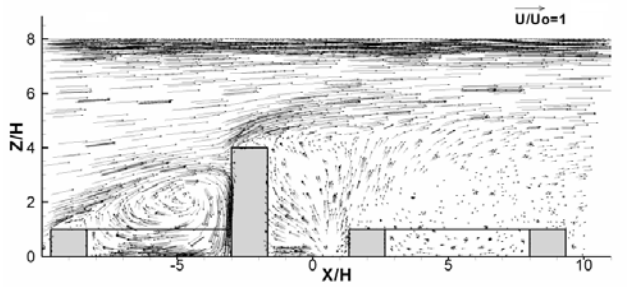

Fig. 6 Mean velocity vectors from CFD at *y/H* = 2.5. Freestream flow is from left to right.

An additional flow feature that in many cases may have significant effects on dispersion is the lateral flow along the avenues toward the tower. This lateral flow supplies air to fill the void created by the vertical flow up the lee side of the tower. This phenomenon can be seen clearly in cross-sectional (or spanwise) views of the measured velocity field in planes perpendicular to the downstream direction. Fig. 7a shows a spanwise view of the flow in the avenue immediately downwind of the tower (at *x/H* = 0). The velocity vectors show lateral flow toward the tower, especially in the lower half of the street canyon. The strength of the lateral movement produces velocities that reach 50% of the freestream velocity in magnitude. The ability of the tower to produce lateral flows in the avenues persists with downstream distance.

Even one block downwind (Fig. 7b, *x/H* = 10.3) the magnitude of the lateral flow reaches 30% of the freestream velocity.

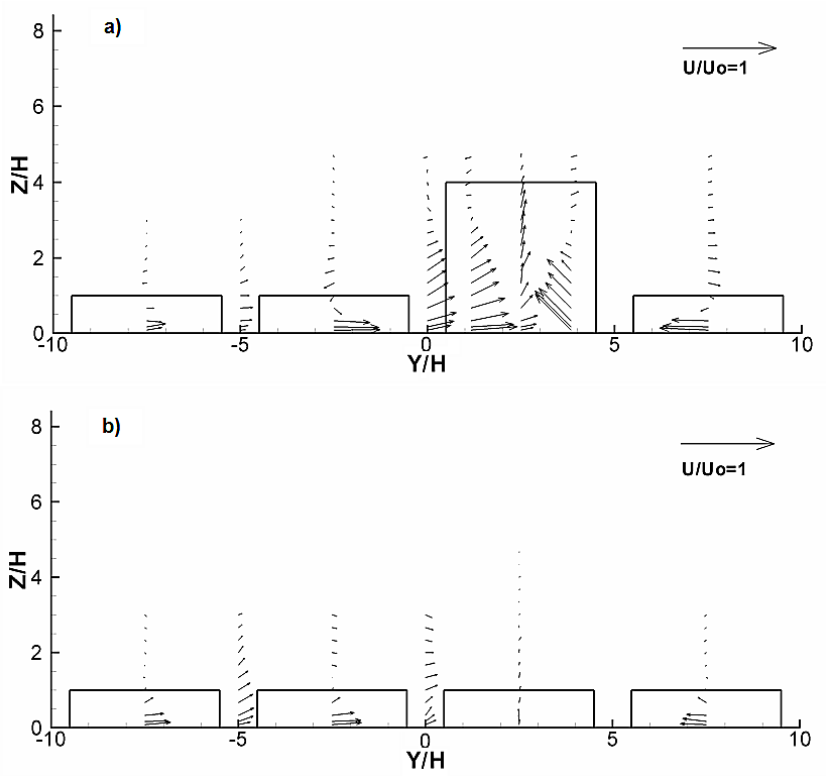

Fig. 7 a) Mean velocity vectors measured with LDV at *x/H* = 0. Note the flow toward the tower in the avenue. The magnitude of the flow velocity is approximately half the freestream velocity. Flow is up the lee side of the tall building. b) Mean velocity vectors measured with LDV at *x/H* = 10.3. One block downstream of the tower strong lateral flow toward the tower persists.

CFD results also show the lateral flow in the avenues. Figs. 8a and 8b present the same cross-sectional views of the flow for the CFD results that Figs. 7a and 7b presented for the wind tunnel results. The CFD results show flow up the leeward side of the tower (Fig. 8a) with two counter-rotating swirls downwind of the tower. The updraft draws air from near ground level, creating a flow toward the tower in the avenue behind the tower. This lateral flow toward the tower extends the full width of the building array. Also visible in Fig. 8a are large swirls of flow behind the lower buildings (counterclockwise to the left of the tower, clockwise to the right) with flow above the buildings in the opposite direction to the flow in the avenue. One block

downwind of the tower (Fig. 8b) the vertical flow has abated, but the flow toward the tower in the avenue persists.

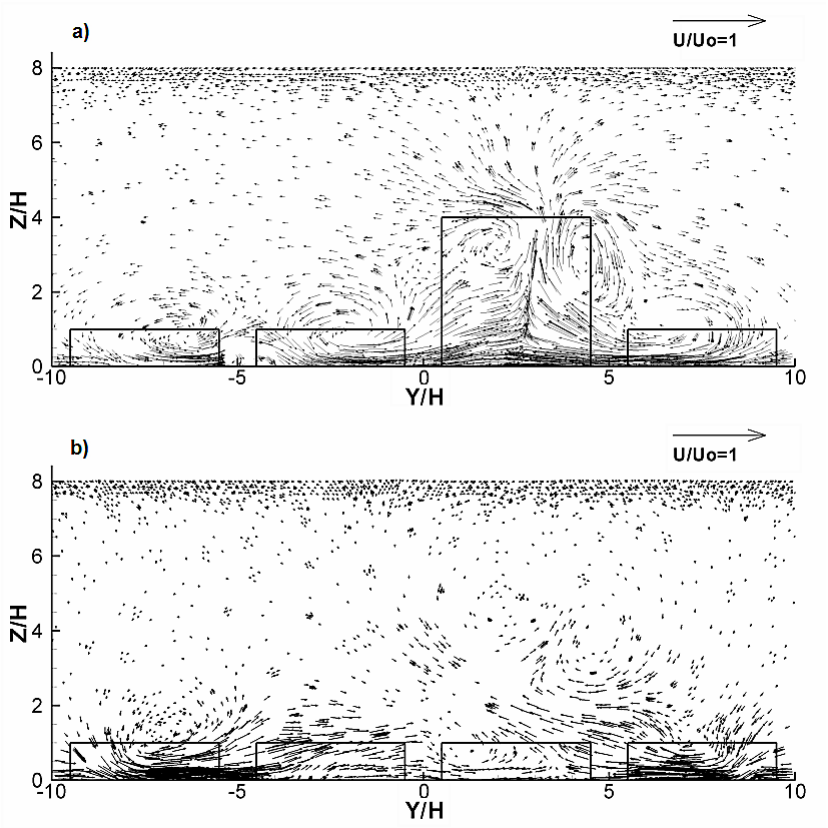

Fig. 8 Mean velocity vectors from CFD at a) *x/H* = 0 and b) *x/H* = 10.5.

A horizontal slice through the street canyons at *z/H* = 0.5 illustrates the interactions between the street and avenue flows (see Fig. 9). Flow proceeds in the downwind direction in the streets (except immediately downwind of the tower) and is partially diverted into the avenues in the intersections. Significant lateral flow toward the tower is seen in the avenue immediately downstream of the tower, as well as in the two downwind avenues. The flows in the streets immediately adjacent to the tower exhibit higher velocities due to the momentum transferred by the downwash on the upstream side of the tower. The velocity near the end of the block in the streets just upwind of Avenue 2 (at *x/H* = -2) is approximately 50–65% higher than at the corresponding location just upwind of Avenue 4, two blocks from the tower. Flow in the streets adjacent to the block just downwind of the tower is nearly stagnant on average.

The numerical simulation shows many of the same features in the street canyons (see Fig. 10). There is a diversion of the flow down the streets into the avenues at the intersections, strong lateral flow in the cross-stream avenues, and acceleration in the flow immediately adjacent to the tower. The flow in the streets adjacent to the block just downwind of the tower exhibits a reversal in direction, flowing against the freestream direction. This phenomenon was substantially less significant in the wind tunnel model. Given the demonstrated accuracy of LES in predicting velocity and turbulence kinetic energy in the wake of rectangular cylinders,[26] this discrepancy is suspected to be due to the small differences in geometry between the two configurations.

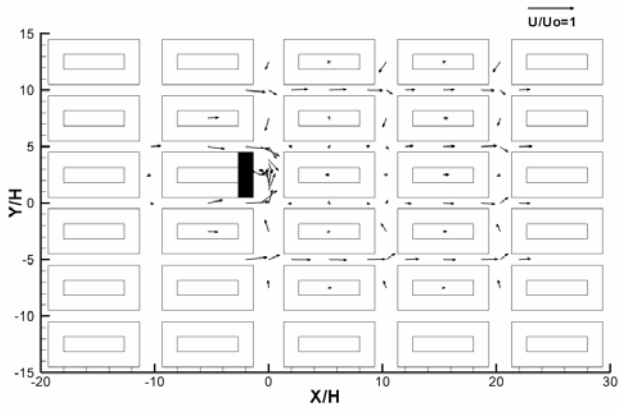

Fig. 9 Mean velocity vectors measured using LDV at *z/H* = 0.5. Lateral flow in avenues persists even to the third avenue. Flow in the street immediately downwind of the tower is inhibited by the presence of the tower. Freestream flow is from left to right.

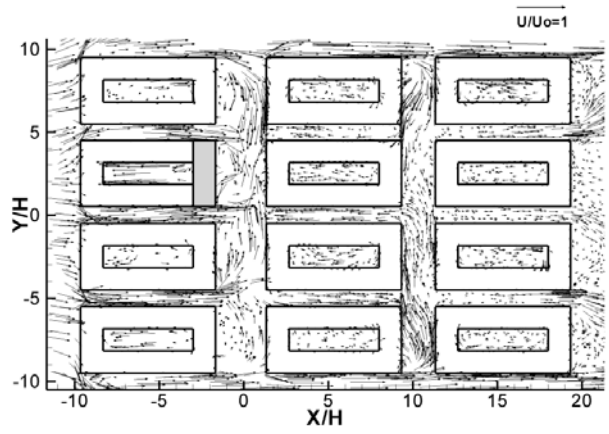

Fig. 10 Mean velocity vectors from CFD at *z/H* = 0.5. Freestream flow is from left to right.

Pressure fields predicted in the numerical simulations are useful in completing the picture of the flow through the city array. Figs. 11a and 11b show the coefficient of pressure (Cp) for two vertical planes, at $y/H = 2.5$ and at $x/H = 0$. In Fig. 11a, the high pressure on the windward side of the building is clearly visible as the flow approaches the tower and decelerates. Pressures at and below $z/H = 1$ were measured in the courtyard on the windward tower face and agree well with the predicted values (measured Cp varied between 0.20 and 0.26 in that area). As seen in Fig. 11b there is a low pressure region directly downstream of the tower that is widest near the rooftop level. This negative pressure region is consistent with the flow in the cross-stream avenues being driven from regions of higher to lower pressures (*i.e.*, toward the tower).

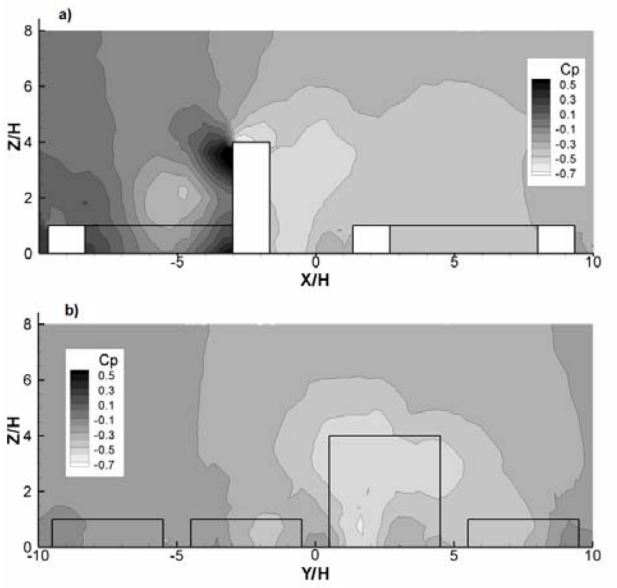

Fig. 11 Coefficient of pressure from CFD in the a) $y/H = 2.5$ plane and b) $x/H = 0$ plane.

Several studies have examined the case of a street canyon with buildings of equal height on the upstream and downstream sides of the street.[27,28] In that case, turbulent transport was found to be the dominant mechanism for ventilation of the street canyon. Liu and Barth[28] note that very little of the pollutant is removed by this mechanism. Others have found poor ventilation of the street canyons for flow through regular arrays of buildings simulating an urban area.[5] Xia and Leung[7] showed in a numerical study that an increase in the height of the buildings, especially upwind of a street canyon, can improve the ventilation rates and reduce local pollutant concentrations when sources are located at ground level in the street canyon. In their study of

two-dimensional buildings, the variation in height of buildings surrounding a street canyon had a great impact on the flow fields in the street canyon, even when the tall building was not adjacent to the street canyon. Our results suggest that the addition of one lone tower in an otherwise uniform array of buildings can have a significant effect on the advection in a street canyon and the resulting ventilation.

The presence of the tall building dramatically affects channeling of flow down the lateral avenues in the building array. These lateral flows have been seen in other circumstances arising from other causes. In some cases, traffic can cause a similar effect. Kastner-Klein *et al.*[3] showed that one-way traffic can act as a piston driving flow in the direction of the traffic with velocities that approach half the wind velocity aloft (at a height of 4*H*). However, with two-way traffic the lateral mean velocities remain nearly unchanged from the case with no traffic, although with higher turbulence levels in the streets. Rafailidis[5] observed lateral flows in street canyons formed by two-dimensional buildings with winds perpendicular to the street, attributing them to minor asymmetries in the physical domain. Leitl and Meroney,[29] in a numerical simulation of the same geometry, traced the source of the lateral flow to the corner vortices at the end plates of the model street canyon. The magnitude of the lateral flow in the simulations, however, seemed to have little effect on pollutant concentrations in the symmetry plane of the street canyon. The lateral flow in the present study, in contrast, significantly affected the plume spread as discussed in Brixey *et al*.[9]

Conclusions

This study illustrates the dramatic effect that tall towers can have in an otherwise uniform array of shorter buildings, enhancing the wind velocities in the street canyons and the ventilation of the street canyon. In the case presented here, the horizontal flow in the street canyons perpendicular to the prevailing winds aloft reached speeds equal to 50% of the freestream wind speed. In the absence of the tower, these are expected to be negligible. In addition, the vertical flow on the downwind side of the tower reached 25% of the freestream wind speed. A low-pressure region was observed in the numerical simulation on the lee side of the tower. The lateral flow in the street canyons is toward this region of low pressure.

The flow that develops as a result of the presence of a tall tower among an otherwise uniform array of shorter buildings has important implications for dispersion of pollutants.

Future research is needed to explore the extent to which the vertical flow induced by a tower is dependent on the existence or configuration of a network of street canyons from which to draw air. A goal of this research would be to find scaling relationships that relate the height or frontal area of the tower to flow velocities within street canyons and up the lee sides of tall buildings.

References

1. M. J. Davidson, K. R. Mylne, C. D. Jones, J. C. Phillips, R. J. Perkins, J. C. H. Fung and J. C. R. Hunt, *Atmos. Environ.,* 1995, **29**, 3245–3256.

2. S. R. Hanna, S. Tehranian, B. Carissimo, R. W. MacDonald and R. Lohner, *Atmos. Environ.*, 2002, **36**, 5067-5079.

3. P. Kastner-Klein, E. Fedorovich and M. W. Rotach, *J. Wind Eng. Indus. Aerodyn.*, 2001, **89**, 849–861.

4. R. W. MacDonald, R. F. Griffiths and D. J. Hall, *Atmos. Environ.*, 1998, **32**, 3845–3862.

5. S. Rafailidis, *Boundary-Layer Meteorol.*, 1997, **85**, 255–271.

6. S. G. Perry, D. K. Heist, R. S. Thompson, W. H. Snyder and R. E. Lawson, *Environ. Manager*, February 2004, 31–34.

7. J. Xia and D. Y. C. Leung, *Atmos. Environ.*, 2001, **35**, 2033–2043.

8. H. Cheng and I. P. Castro, *Boundary-Layer Meteorol.*, 2002, **104**(2), 229–259.

9. L. A. Brixey, J. Richmond-Bryant, D. K. Heist, G. E. Bowker, S. G. Perry and R. W. Wiener, The effect of a tall tower on flow and dispersion through a model urban neighborhood, Part 2. pollutant dispersion, 2007, in review.

10. Z. E. Drake-Richman, L. A. Brixey, S. Lee, C. R. Fortune, A. D. Eisner, J. Richmond-Bryant, I. Hahn, W. D. Ellenson and R. W. Wiener, Precision and accuracy tests of the TSI P-Trak real-time ultrafine particle counter, 2007, in review.

11. J. Richmond-Bryant, I. Hahn, C. R. Fortune, C. E. Rodes, S. Lee, J. W. Portzer, R. Baldauf, M. Wheeler, J. Seagraves, M. Stein, Z. E. Drake-Richman, L. A. Brixey, A. D. Eisner, W. D. Ellenson and R. W. Wiener, The Brooklyn Traffic Real-Time Ambient Pollutant Penetration and Environmental Dispersion (B-TRAPPED) Study, 2007, in review.

12. J. Richmond-Bryant, A. D. Eisner, I. Hahn, C. R. Fortune, Z. E. Drake-Richman, L. A. Brixey, M. Talih, W. D. Ellenson and R. W. Wiener, Time-series analysis to study the impact of an intersection on dispersion along a street canyon, 2007, in review.

13. A. D. Eisner, J. Richmond-Bryant, I. Hahn, Z. E. Drake-Richman, L. A. Brixey, W. D. Ellenson and R. W. Wiener, Analysis of indoor air pollution trends and characterization of infiltration delay time using a cross-correlation method, 2007, in review.

14. A. D. Eisner, J. Richmond-Bryant, I. Hahn, Z. E. Drake-Richman, W. D. Ellenson and R. W. Wiener, Establishing a link between vehicular PM sources and PM measurements in urban street canyons, 2007, in review.

15. W. H. Snyder, The EPA Meteorological Wind Tunnel: Its Design, Construction, and Operating Characteristics, Report No. EPA-600/4-79-051, U. S. Environmental Protection Agency, Research Triangle Park, NC, 1979.

16. H. P. A. H. Irwin, *J. Wind Eng. Indus. Aerodyn.*, 1981, **7**, 361–366.

17. W. H. Snyder, Guideline for Fluid Modeling of Atmospheric Diffusion, Report No. EPA-600/8-81-009, U. S. Environmental Protection Agency, Research Triangle Park, NC, 1981.

18. P. J. Roache, *Verification and Validation in Computational Science and Engineering,* Hermosa Publishers, Albuquerque, NM, 1998.

19. E. S. P. So, A.T. Y. Chan and A. Y. T. Wong, *Atmos. Environ.*, 2005, **39**, 3573–3582.

20. A. Walton, A. Y. S. Cheng and W. C. Yeung, *Atmos. Environ.*, 2002, **36**, 3601–3613.

21. C.-H. Liu, D. Y. C. Leung and M. C. Barth, *Atmos. Environ.*, 2005, **39**, 1567–1574.

22. Y.-H. Tseng, C. Meneveau and M. B. Parlange, *Environ. Sci. Technol.*, 2006, **40**, 2653–2662.

23. P. J. Mason, *Quart. J. Royal Met. Soc.*, 1994, **120**, 1–26.

24. J. Smagorinsky, *Mon. Wea. Rev.*, 1963, **91**, 99–164.

25. D. K. Lilly, On the application of the eddy viscosity concept in the inertial subrange of turbulence, NCAR Manuscript 123, 1966.

26. H. Lübcke, St. Schmidt, T. Rung and F. Thiele, *J. Wind Eng. Ind. Aerodyn*, 2001, **89**, 1471-1485.

27. J.-J. Baik and J.-J. Kim, *Atmos. Environ.*, 2002, **36**, 527–536.

28. C.-H. Liu and M. C. Barth, *J. Appl. Meteorol.*, 2002, **41**, 660–673.

29. B. M. Leitl and R. N. Meroney, *J. Wind Eng. Indus. Aerodyn*., 1997, **67–68**, 293–304.